

Characterizing effects of humidity and channel size on imbibition in paper-based microfluidic channels

Carlos Castro^{1,4} · Cindy Rosillo¹ · Hideaki Tsutsui^{1,2,3}

Received: 26 September 2016 / Accepted: 16 January 2017 / Published online: 2 February 2017
© Springer-Verlag Berlin Heidelberg 2017

Abstract Paper-based microfluidic devices have gained an increasing amount of interest over the last few years. As such devices continue advancing toward more complex and sophisticated functions, obtaining accurate and consistent fluid imbibition under different conditions will become increasingly important. This study presents a series of controlled imbibition experiments investigating effects of relative humidity and channel width in paper-based microfluidic channels. The obtained imbibition data highlighted the importance in accounting for the effects of these design and environmental parameters. Additionally, fitting of the experimental data to three relevant imbibition models revealed evaporation, not water saturation, to be the main mechanism of the observed relative humidity effect. The current study has created a library of paper-specific, imbibition-related properties for commonly used filter and chromatography papers for the first time. Collectively, the presented imbibition data and the discovered relationships

are expected to help researchers design more precise and reproducible paper-based microfluidic devices.

Keywords Paper-based microfluidics · Wicking · Imbibition · Relative humidity

1 Introduction

Paper-based microfluidics has generated a great amount of interest for the development of diagnostic and self-contained analytical devices. Applications range from health-care, food safety, environmental monitoring, among others. What has in part attracted attention is the low-cost, ease-of-use, and adaptability of these paper devices. Compared to conventional microfluidic devices, the paper-based counterparts are able to utilize paper's inherent wicking property to eliminate the external pumping needed to drive the fluid. Channels are easily formed by either selectively removing sections of the paper substrate or by patterning channel boundaries with a hydrophobic material. The former methods range from using high-precision CO₂ laser-cutting (Chitnis et al. 2011; Fu et al. 2010) to craft cutting (Fenton et al. 2009), while the latter methods range from those of photolithography (Martinez et al. 2008b) to techniques using commercially available printers with inkjet (Abe et al. 2010) or solid ink (Carrilho et al. 2009) technology. Ultimately, the common result of these fabrication methods is the creation of a defined impermeable boundary for fluid transport. Thorough reviews on fabrication methods have recently been published (Cate et al. 2015a; Jiang and Fan 2016; Xia et al. 2016; Yetisen et al. 2013). In spite of the benefits and advantages described above, paper-based microfluidic technologies often lack the necessary sensitivity and sophistication available in conventional microfluidic

Electronic supplementary material The online version of this article (doi:10.1007/s10404-017-1860-4) contains supplementary material, which is available to authorized users.

✉ Hideaki Tsutsui
htsutsui@engr.ucr.edu

¹ Department of Mechanical Engineering, University of California, Riverside, Riverside, CA 92521, USA

² Department of Bioengineering, University of California, Riverside, Riverside, CA 92521, USA

³ Stem Cell Center, University of California, Riverside, Riverside, CA 92521, USA

⁴ Present Address: Mechanical Engineering Department, California State Polytechnic University, Pomona, Pomona, CA 91768, USA

devices. In order to be a competitive alternative, paper-based microfluidics requires improvement and novel development of feasible detection methods. These methods will likely require increasingly complex chemistry and control of reagents. Thus, obtaining precise, accurate, and consistent fluid handling within the paper device will be crucial.

Currently, the most widely used imbibition model in the paper-based microfluidic community is the Lucas–Washburn (L–W) equation (Lucas 1918; Washburn 1921) where the progression of the imbibition front is taken to be proportional to the square-root of time. More extensive theoretical models for imbibition as well as fluid front concentration gradients in analyte transport (Berli and Kler 2016) are available from the porous media research community. These imbibition models include models derived from diffusion dynamics (Richards 1931), models that include fluctuations created by the roughness of the material (Krug and Meakin 1991), and models based on statistical methods (Kardar et al. 1986), among others (Alava et al. 2004). These models are valuable and used to understand the detailed dynamics occurring within and during the imbibition process. However, practical implementation of these models under the context of paper-based microfluidic devices is lacking mainly due to the extensive empirical model parameters required to reproduce the highly dynamic imbibition phenomena. Consequently, the L–W model is still widely used by the paper-based microfluidic community due to its simplicity, ease-of-use, and adequate accuracy for the current characterization needs. The L–W equation has been used to compare superabsorbent material to laboratory-grade filter paper (Schuchardt and Berg 1991), used to design simple sequential delivery devices (Fridley et al. 2014; Fu et al. 2010; Lutz et al. 2013), and to characterize wettability of modified paper (Bohm et al. 2014; Li et al. 2010; Lutz et al. 2013). Even though the L–W equation is arguably the standard in paper-based microfluidics, for the field to continue advancing toward more sophisticated and precise device functions, it is imperative that better knowledge in and tools for characterization of the liquid imbibition be available to researchers.

One of the primary applications of paper-based microfluidics is analyte detection. Various flow control methods have been investigated in order to provide the necessary fluid handling for the varying degree of detection processes. These processes can range from simple glucose detection (Martinez et al. 2007) or signal amplification (Fu et al. 2010) to more complex processes where sequential and timed handling of the fluid sample and reagents are required such as with enzyme-linked immunosorbent assay (ELISA) (Apilux et al. 2013) and with “paper machines” where fluid handling is integrated with loop-mediated isothermal amplification (LAMP) (Connelly et al. 2015). Methods to control imbibition include changing the channel geometry and the

physical properties of the paper. Several groups have investigated and proposed several cross-sectional geometries. The Yager group investigated the wet-out and fully wetted flows in 2-D channel networks (Fu et al. 2011; Kauffman et al. 2010), Mendez et al. (2010) studied fan-shaped expansion channels that can induce quasi-steady-state flows in the preceding straight channel section, Shou et al. (2014) investigated contraction/expansion segments along the channel, and Elizalde et al. (2015) proposed a general expression for continuous cross-sectional change in geometry as a way to control fluid flow. In addition to geometrical manipulation of the paper channel, modifying and adjusting the permeability of the paper have also been shown to be effective. These methods among others include using hydrophobic polymers (Bohm et al. 2014; Noh and Phillips 2010; Weng et al. 2014), using dissolvable and erodible barriers (Jahanshahi-Anbuhi et al. 2014; Lutz et al. 2013), as well as physical methods such as compressing paper (Park et al. 2016) and selectively cutting the paper (Giokas et al. 2014; Renault et al. 2013). Although considerable knowledge exists on techniques to manipulate fluid within the paper channel, what is lacking are studies on how non-laboratory conditions (e.g., relative humidity) influence fluid flow. An exception is a very recent study by Walji and MacDonald (2016) where the authors experimentally investigated effects of the paper channel geometry and surrounding conditions.

In the present study, we focus on the effects of relative humidity and channel width to help address this knowledge gap further. We report a series of controlled imbibition experiments using cellulose papers commonly used in the field of paper-based microfluidics. We show that both the imposed relative humidity and the channel width have critical design considerations in paper-based devices. Additionally, we compare three models, the L–W model, the Fries et al. (2008) model which incorporates evaporation, and a newly developed water saturation model. We assess their accuracy in representing the experimental data and systematically evaluate the importance of evaporation and water saturation under a wide range of relative humidity conditions.

2 Materials and methods

2.1 Material and device fabrication

Four different paper types were surveyed in this study: Whatman qualitative filter paper of Grade #1 (Cat. No. 1001-185; Lot No. FC009260), Grade #4 (Cat. No. 1004-185; Lot No. FC005565), Grade #5 (Cat. No. 1005-185; Lot No. 9463409), and Whatman chromatography (Chr) paper of Grade 1 (Cat. No. 3001-861; Lot No. FS005173) (GE Healthcare, Pittsburgh, PA). Based on the distance wicked over time, the paper types can be classified into

three qualitative imbibition speeds (slow, medium, and fast). The test device and the specified paper pieces' dimensions were designed in SolidWorks (Dassault Systèmes, Vélizy-Villacoublay, France) and cut using a Zing 16 CO₂ laser cutter (Epilog Laser, Golden, CO). All wetting and imbibition experiments were conducted using ultrapure water (18.2 MΩ-cm) prepared by a Millipore Synergy UV water purification system (Billerica, MA). Relevant properties of the surveyed papers are summarized in Table 1. An ambient temperature of 25 ± 0.5 °C was maintained throughout the experiments in this study.

2.2 Characterization of evaporation flux

Evaporation flux was experimentally measured in two ways as described below: evaporation from a fixed pre-wetted area (static evaporation) and evaporation from a dynamically wetted area (dynamic evaporation).

In the static evaporation experiment, a 40 × 40 mm laser-cut piece of paper was hung on an analytical scale (Model TP-64, Denver Instrument, Bohemia, NY) placed inside an environmentally controlled chamber (Model 5503-E, Electro-Tech Systems, Glenside, PA). Preliminary studies showed that the lowest possible relative humidity that could be maintained during the imbibition process with a water reservoir inside was 18% (without the water reservoir, 3% was the lowest achievable). The chamber was set to a specified relative humidity value (18, 25, 50, 75, 90, or 99%) and left for an hour to allow the paper piece to reach equilibrium with the chamber environment. The paper was then wetted by evenly applying water using a micropipette. 0.25 mL of water fully wetted the sample without visible excess water accumulating at the edges. The mass of the paper was recorded as water evaporated over 30 min, while relative humidity was maintained at the designated value. This experiment was repeated five times for each relative humidity value and each paper type. The rate of evaporated water mass was divided by the total surface area of the paper piece to calculate the evaporation flux, F .

In the dynamic evaporation experiment, the evaporation rate was measured from a laser-cut piece of paper (50 × 150 mm) undergoing the imbibition process on top of an analytical scale. The relative humidity was set to 25, 50,

and 75%. The evaporation flux was calculated using the rate of water evaporation from the piece of paper and the changing surface area of the wetted region. Similarly to the static evaporation experiments, measurements were repeated five times for each relative humidity value and each paper type.

2.3 Characterization of residual water

A 70 × 70 mm laser-cut piece of paper was put in an open glass container and dried at 105 °C for 1 hour in a convection oven (Model FD-53, Binder, Bohemia, NY). The glass container was then immediately sealed with a dry lid and transferred to the environmentally controlled chamber. Once the chamber reached its lowest possible relative humidity value (3%), the paper sample was taken out and immediately placed on the analytical scale to measure its dry mass. The paper strip was then hung on the scale and left for an hour at a specified relative humidity value (10, 18, 25, 50, 75, 90, or 99%) to reach equilibrium before its mass was measured and recorded. Ten replicates were tested for each relative humidity value and each paper type. Based on the dry mass of paper, the amount of water retained (i.e., volume fraction of residual water) in the unwet paper, here called water saturation S_w , was calculated for each relative humidity. See Section S3 of electronic supplementary information for detail.

2.4 Measurement of imbibition distance

The paper device was mounted vertically on the test fixture inside the environmentally controlled chamber (Fig. 1a, b). As shown in Fig. 1c, each device features 41-mm-long channels of 1, 2, 4, 10, and 20 mm widths. A water reservoir was placed on a laboratory jack (Model L-490, Thorlabs, Newton, NJ). The jack's platform was then raised quickly to the start line of the channels. The imbibition process was recorded using a Nikon D5100 digital camera (Tokyo, Japan). Image frames were then extracted from the recorded video files using Adobe Premiere Pro CS6 (San Jose, CA). Image brightness was adjusted digitally to increase the contrast of the imbibition front. Imbibition distance was then measured at the centerline position of the liquid front using ImageJ with the Manual Tracking

Table 1 Properties of the surveyed paper types in the current study

Paper type (speed)	Density of cellulose fiber, ρ_c	Thickness ^a , T (μm)	Basis Weight ^a , W_B (g/m ²)	Porosity ^a , ϕ
Whatman #1 (Medium)	1500–1600 kg/m ³	180	81.71	0.707
Whatman #4 (Fast)	(Bledzki and Gassan 1999; Moon et al. 2011)	205	83.96	0.736
Whatman #5 (Slow)		200	92.35	0.702
Whatman Chr-1 (Medium)		180	81.98	0.706

^a See electronic supplementary information for detail

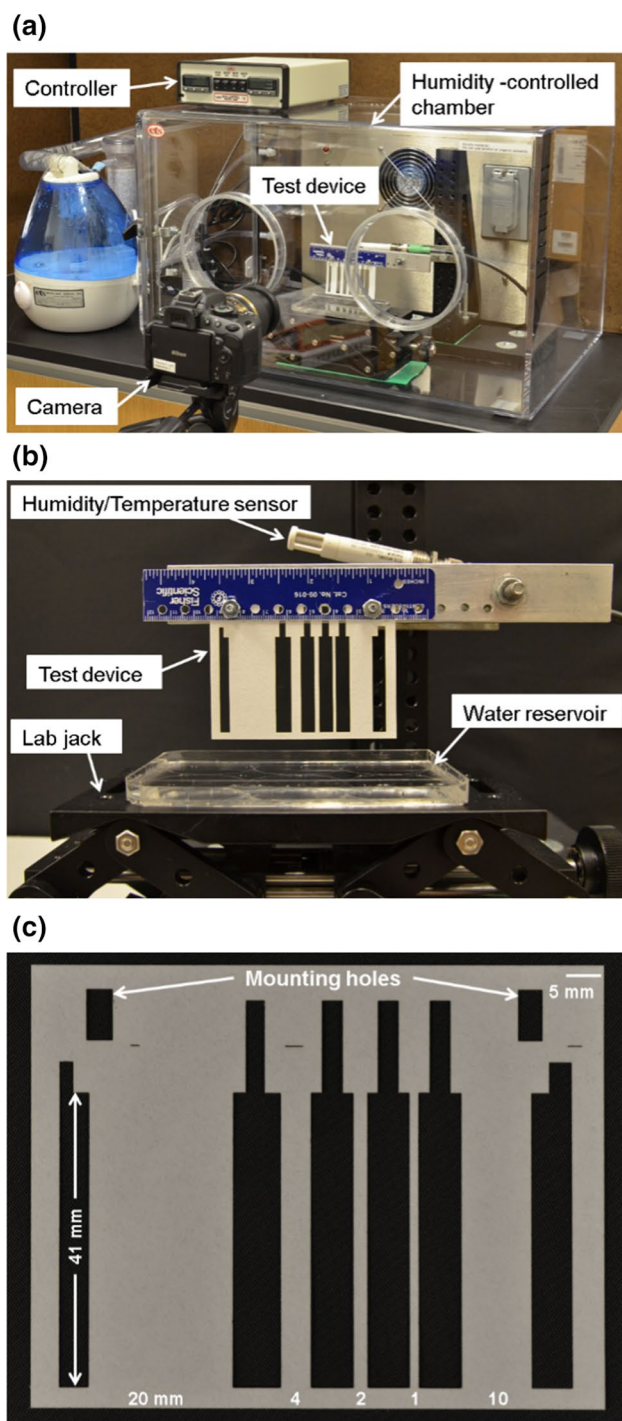


Fig. 1 Test setup for imbibition experiments. **a** Overview of test setup. A pair of gloves (not shown) were attached to the glove ports and used during the experiments to access the sample and the laboratory jack. **b** Close-up view of the testing section. **c** An unmounted paper device featuring 5 channels of 1, 2, 4, 10, and 20 mm width

plug-in. Ten replicates were tested for each combination. The combinations include variations in channel width (1, 2, 4, 10, 20 mm), relative humidity (18, 25, 50, 75, 90, and 99%), and paper type (Whatman #1, #4, #5, and Chr-1).

2.5 Calculation of effective permeability

A custom MATLAB script was written and used to calculate effective permeabilities, K , of the L–W model, the Fries et al. model, and the water saturation model by curve fitting against the experimentally obtained imbibition data. The effective permeability value was chosen based on the highest R^2 value.

3 Results and discussion

3.1 Imbibition studies

An array of imbibition studies was conducted to explore a wide range of imbibition scenarios. These scenarios included combinations of five different channel widths (1, 2, 4, 10, and 20 mm), four commonly used paper types (Whatman #1, #4, #5, and Chr-1), and six different relative humidity values (18, 25, 50, 75, 90, and 99%). Figure 2 shows imbibition distance versus time for different channel widths at selected relative humidity values for each surveyed paper (complete set available in Fig. S6–S9).

Within each paper type, two relations were consistently observed. First, the imbibition distance at a specified time increased as relative humidity increased. For example, to reach a height of 40 mm with a 2-mm-wide channel the relative humidity can delay the liquid front by as much as 60–800 s depending on the type (speed) of the Whatman paper. This demonstrates the strong inhibitory effect of low relative humidity on liquid imbibition. The second observed relation corresponds to the channel width. For a specified relative humidity, the liquid front travels less distance for narrow channels after an elapsed time and becomes less pronounced as the channel width increases. This channel width effect decreases as the relative humidity increases. The channel width dependence on imbibition has previously been observed in channels with hydrophobic boundaries. The inhibitory effect is suggested to be caused when the fiber length is larger than the width of the channel, terminating the flow at the side edges of the channel (known as dead-end pores) (Bohm et al. 2014) or caused by the increase in contact angle seen at the wall (Hong and Kim 2015). Nonetheless, a narrow channel has an increased resistance, with an asymptotic plateau for wider channels. Interestingly, the dependence in both relative humidity and channel width is more pronounced in slower wicking papers. In an extreme case, 1-mm channels of Whatman #5 (slow wicking) could not be fully wicked at 18% relative humidity because the liquid front was pinned at around 30 mm distance (Fig. 2c). The pinning can be caused by a combination of low permeability of paper, dead-end pores, and strong evaporation. Balankin et al. (2013) found that

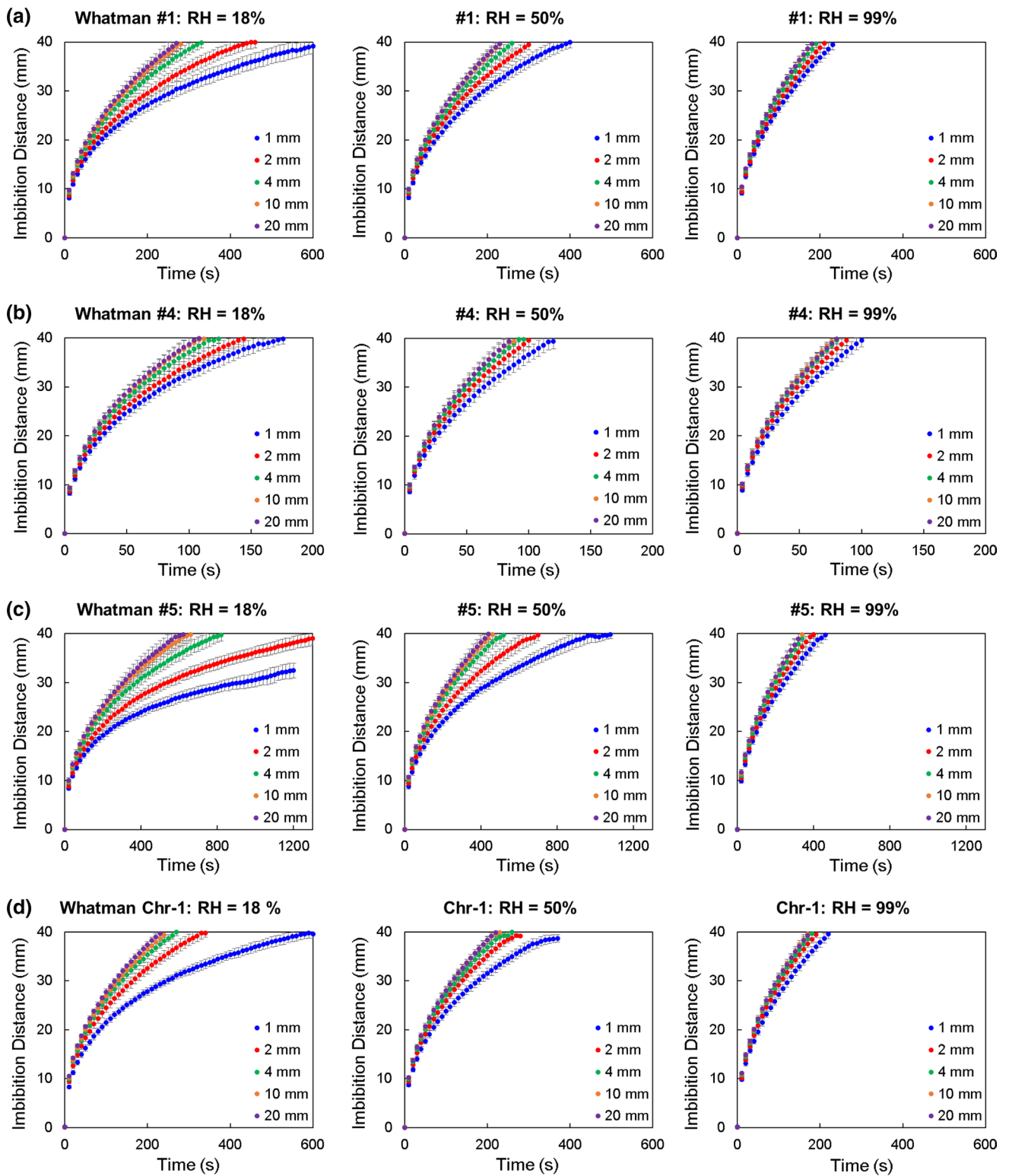


Fig. 2 Imbibition distance versus time of surveyed paper types at selected relative humidity: **a** Whatman #1, **b** Whatman #4, **c** Whatman #5, and **d** Whatman Chr-1. Channel width tested: 1, 2, 4, 10, and 20 mm. Data shown as mean \pm SD ($N = 10$)

if there is a rapid increase in relative humidity, the once pinned front could be unpinned.

3.2 Imbibition modeling

A detailed description of imbibition becomes increasingly complicated as the parameters involved are frequently time- and length-scale dependent. These parameters, among others, include properties involving pore size, porosity, tortuosity, contact angle, the degree of swelling, and roughening terms describing perturbations of liquid front. Extensive studies have been done to understand the underlining imbibition dynamics, and sophisticated models have been derived from diffusion theory (Richards 1931), stochastic theory (Kardar et al. 1986), and percolation theory (Amaral et al. 1995). However, the shared trait among these advanced models is the large number of parameters and theoretical constants needed, often requiring fit to the specific situation to be addressed. Even analytically friendly models incorporating swelling are case specific, and swelling parameters need fitting to the experimental data (Masoodi and Pillai 2010). For practical characterization and usage in the paper-based microfluidics field, more user-friendly models are preferred.

The current standard for paper-based microfluidic modeling is the L–W model (Eq. 1), a simple imbibition model derived by combining capillary theory with Hagen–Poiseuille flow (Lucas 1918; Washburn 1921), where the substrate is assumed as a bundle of capillary tubes with an infinite reservoir. Though known to be theoretically inaccurate in describing the imbibition flow (Alava et al. 2004), the L–W equation is frequently used as a first-order approximation due to the very good empirical description of the liquid front and the ease-of-use. The liquid front is described by,

$$y_f = \sqrt{\frac{D_e \gamma \cos \theta}{4\mu}} t, \quad (1)$$

where y_f is the imbibition distance of the liquid front, D_e is the effective capillary diameter, γ is the surface tension of the liquid, θ is the capillary contact angle, μ is the dynamic viscosity, and t is the imbibition time. Since the L–W model is only dependent on effective material pore and the liquid properties, it predicts that any channel width will have the same imbibition behavior. However, the simple characterization attributes associated with the L–W equation can be invalidated in non-ideal laboratory settings, such as imbibition in different relative humidity. This specific issue raises questions and concerns about relative humidity effects such as evaporation and water saturation. Therefore, there is a need in the paper-based microfluidic field to characterize such possible effects in a straight forward manner and with approachability.

To characterize the imbibition front of all surveyed combinations and to assess the importance of relative humidity, we compare three models, the L–W model, the Fries et al. (2008) model which incorporates evaporation, and a newly developed water saturation model, where evaporation and residual water are incorporated.

The Fries et al. model stems from the need of an evaporation-based model. Originally derived for metal weaves, the Fries et al. model results in a relatively simple, straight forward imbibition equation that takes evaporation into account.

$$y_f = \left[\frac{a - a \exp(-2bt)}{b} \right]^{\frac{1}{2}}$$

$$a = \frac{K\gamma \cos \theta}{D_e \phi \mu}, \quad b = \frac{F(W + T)}{\phi \rho WT}, \quad (2)$$

where D_e is the effective pore diameter, K is the effective permeability, ϕ is the porosity of the material, F is the evaporation flux, ρ is the liquid density, W is the channel width, and T is the paper thickness.

Paper, unlike metal weaves, is hygroscopic by nature and will absorb moisture at high relative humidity. Accounting for this, we developed a model that includes residual water associated with the relative humidity. The resulting model (see electronic supplementary information for derivation) is a modified version of the Fries et al. model accounting for the internal volume changes due to the residual water. With gravitational effects being negligible, the implicit model simplifies to Eq. 3, herein called the water saturation model,

$$y_f = \left[\frac{a - a \exp(-2bt)}{b} \right]^{\frac{1}{2}}$$

$$a = \left(\frac{K}{2\phi} \right)^{1/2} \frac{\gamma \cos \theta}{\mu}, \quad b = \frac{F(W + T)}{\phi \rho (1 - S_w) WT}, \quad (3)$$

where S_w is the degree of water saturation.

To compare Eq. 3 to the L–W model and the Fries et al. model, Hagen–Poiseuille and Darcy flows are related so as to produce an alternative form of the L–W equation,

$$y_f = \sqrt{\left(\frac{2K}{\phi} \right)^{1/2} \frac{\gamma \cos \theta}{\mu}} t \quad (4)$$

Similarly, the Fries et al. model becomes,

$$y_f = \left[\frac{a - a \exp(-2bt)}{b} \right]^{\frac{1}{2}}$$

$$a = \left(\frac{K}{2\phi} \right)^{1/2} \frac{\gamma \cos \theta}{\mu}, \quad b = \frac{F(W + T)}{\phi \rho WT}. \quad (5)$$

It is to be noted that when evaporation is zero ($F = 0$) both Eq. 3 and Eq. 5 reduce to the L–W model (Eq. 4), process of which is described in Section S6 of electronic supplementary information (Eq. S20 and S21).

3.3 Evaporation flux

The evaporation flux, F in both Eq. 3 and Eq. 5, was modeled as being constant. To determine this value, a static evaporation flux was calculated by measuring the mass of evaporated water over time under different relative humidity and paper type. Figure S1 shows the linear relationships between mass evaporation and time among all relative humidity/paper combinations. The linear relationship confirms that at constant relative humidity the rate of evaporation (i.e., slope of the plot divided by area) from a constant area is constant irrespective of the wetness of the paper. The only exception was when the majority of the water is evaporated. The nonlinearity is seen during the last 5 min of 18% relative humidity (Fig. S1). At this instant, the four surveyed papers contained at most 5% of the 0.25 mL water added. This results in an approximate liquid-to-surface-area ratio of 8 nL/mm² after 30 min at 18% relative humidity. Since the longest imbibition time was approximately 22 min (see Fig. 2), the linear approximation for 18% relative humidity was assumed. The evaporation flux versus relative humidity is plotted in Fig. 3 with a linear best-fit line for each paper type. As shown, for all paper types the evaporation flux is almost identical with a linear decline as the relative humidity increases.

The assumption of constant evaporation flux in Eqs. 3 and 5 makes the usage of the models more user-friendly. As the paper undergoes the imbibition process, the continuously increasing wetted area might lead to a dynamic

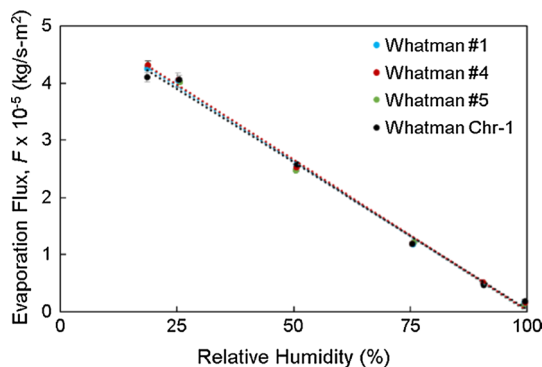


Fig. 3 Static evaporation flux versus relative humidity of surveyed paper types with linear fit (mean $R^2 = 0.9965$). Data shown as mean \pm SD ($N = 5$)

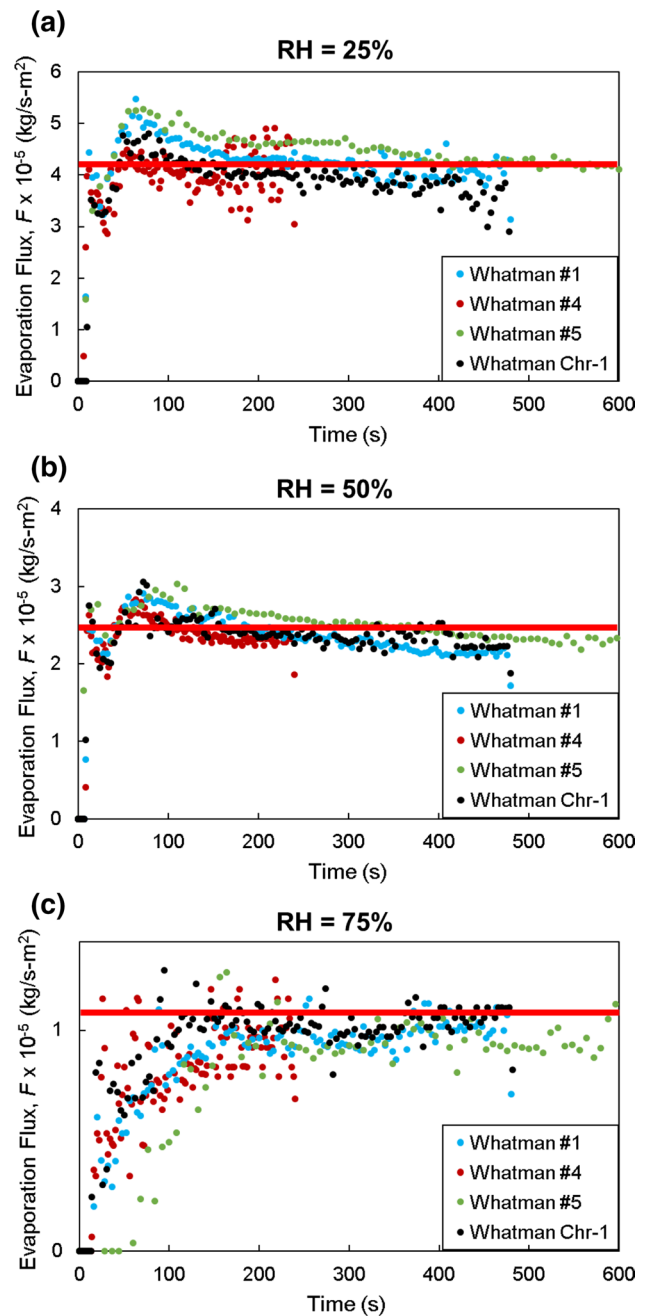


Fig. 4 Dynamic evaporation flux of surveyed paper types versus time. A red horizontal line shows the average static evaporation flux value of the four paper types at the specified relative humidity. Data shown as mean ($N = 5$)

evaporation process. Similar to the static evaporation results, in the dynamic evaporation experiment the four surveyed papers exhibited similar evaporation fluxes at each relative humidity (Fig. 4). The dynamic behavior was seen more explicitly at the higher relative humidity (i.e., 75%). Interestingly, the evaporation flux approached and reached the static evaporation flux values observed in

Fig. 3. Because of the relatively fast asymptotic approach of the dynamic evaporation flux to the static value, as well as the decreasing amount of evaporation with higher relative humidity, we concluded that the static flux values represented evaporation during imbibition reasonably well and therefore used in the subsequent imbibition analysis.

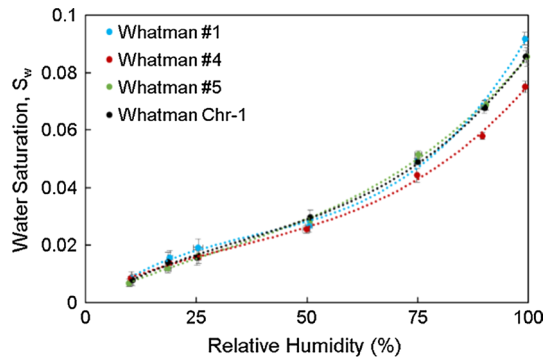


Fig. 5 Water saturation versus relative humidity of surveyed paper types with a cubic fit (mean $R^2 = 0.9986$). Data shown as mean \pm SD ($N = 10$)

3.4 Water saturation

The degree of residual water (i.e., water saturation) at specified relative humidity can be particularly important when it comes to paper due to the hygroscopic nature of cellulose. Figure 5 shows the calculated water saturation S_w for each paper type at relative humidity of 10, 18, 25, 50, 75, 90, and 99%. For each relative humidity, water saturation was observed to be similar across the surveyed paper types up to about 50% relative humidity. Above 50%, the Whatman #4 had noticeably less water saturation than the others. This can be due in part to the relatively large porosity of this specific paper (Table 1; Fig. S4). Higher porosity not only makes the denominator of S_w larger, but also potentially makes the numerator small because a large porosity means less fiber material by which water can be absorbed (see Section S3 of electronic supplementary information). Accordingly, S_w can be noticeably lower for paper with slightly higher porosity (i.e., Whatman #4) than the others. Water retention at 99% relative humidity resulted in a maximum water saturation of 7.5% for Whatman #4 and about 9% for the other three paper types.

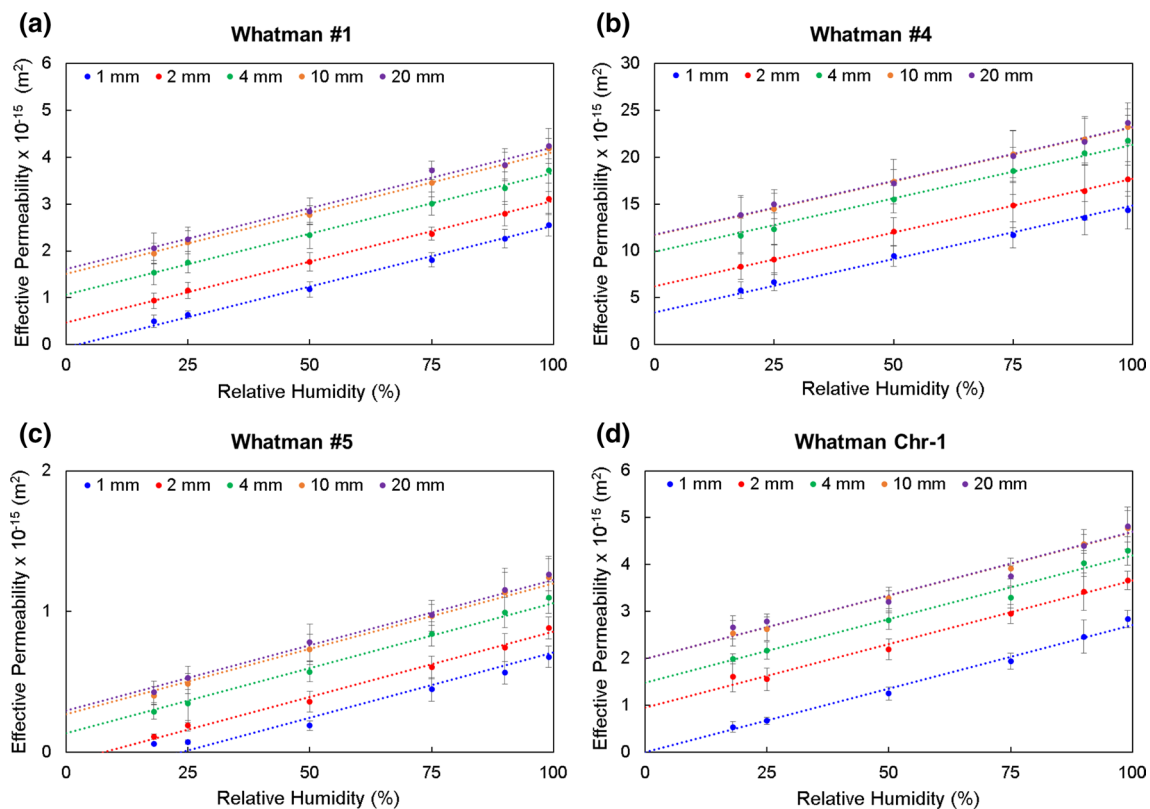


Fig. 6 Effective permeability versus relative humidity of surveyed paper types for the L–W model. **a** Whatman #1, **b** Whatman #4, **c** Whatman #5, and **d** Whatman Chr-1. Dotted lines are best-fit lines with a constant slope. Data points shown as mean \pm SD ($N = 10$)

3.5 Effective permeability and model comparison

The effective permeability, K , of the channel was determined as a way to characterize the observed imbibition behavior. The effective permeability for each scenario (channel width, relative humidity, paper type) was extracted by fitting the L–W model (Eq. 4), the Fries et al. model (Eq. 5), and the water saturation model (Eq. 3) to the imbibition distance versus time data (see electronic supplementary information for the complete set). It should be noted that the L–W model is inherently independent of channel width and relative humidity, but here it was fitted to each scenario. This allowed for a direct comparison of the three models. Because of paper’s high affinity to water and the highly dynamic contact angle within the porous media, the water-paper interface was taken as perfectly wetting ($\theta = 0^\circ$) (Ballerini et al. 2011; Liukkonen 1997; Songok et al. 2014).

The resultant effective permeabilities for each paper type were plotted as a function of relative humidity (Figs. 6, 7, 8). Direct comparisons between the models show that the permeabilities are higher with the inclusion of the evaporation term, in particular, at low relative humidity. A linear relationship with a positive constant slope was observed,

irrespective of the channel width and model. Additionally, the effective permeability asymptotically approached an upper limit with the increasing channel width. These simple practical relationships that are conserved across different paper types can be used by researchers to design better paper devices. Specifically, by knowing the slope and the intercept in the vertical axis (see Table S1, S2, and S3), the imbibition behavior can be easily calculated for a specific paper type, a specific channel width, and a relative humidity value.

Comparing the effective permeability associated with the L–W model (Fig. 6) to either the Fries et al. model (Fig. 7) or the water saturation model (Fig. 8) shows the importance of evaporation, particularly the high evaporation rate that occurs at low humidity. Without a designated term for evaporation, the effective permeability in the L–W model must account for the slowing of imbibition due to evaporation. Differences in the models become less apparent as the relative humidity increases because of the reduced evaporation. This results in a convergence of the L–W model (Eq. 4) and the evaporation models (Eqs. 3 and 5).

In comparing the accuracy in these effective permeabilities, the coefficient of determination, R^2 , was investigated.

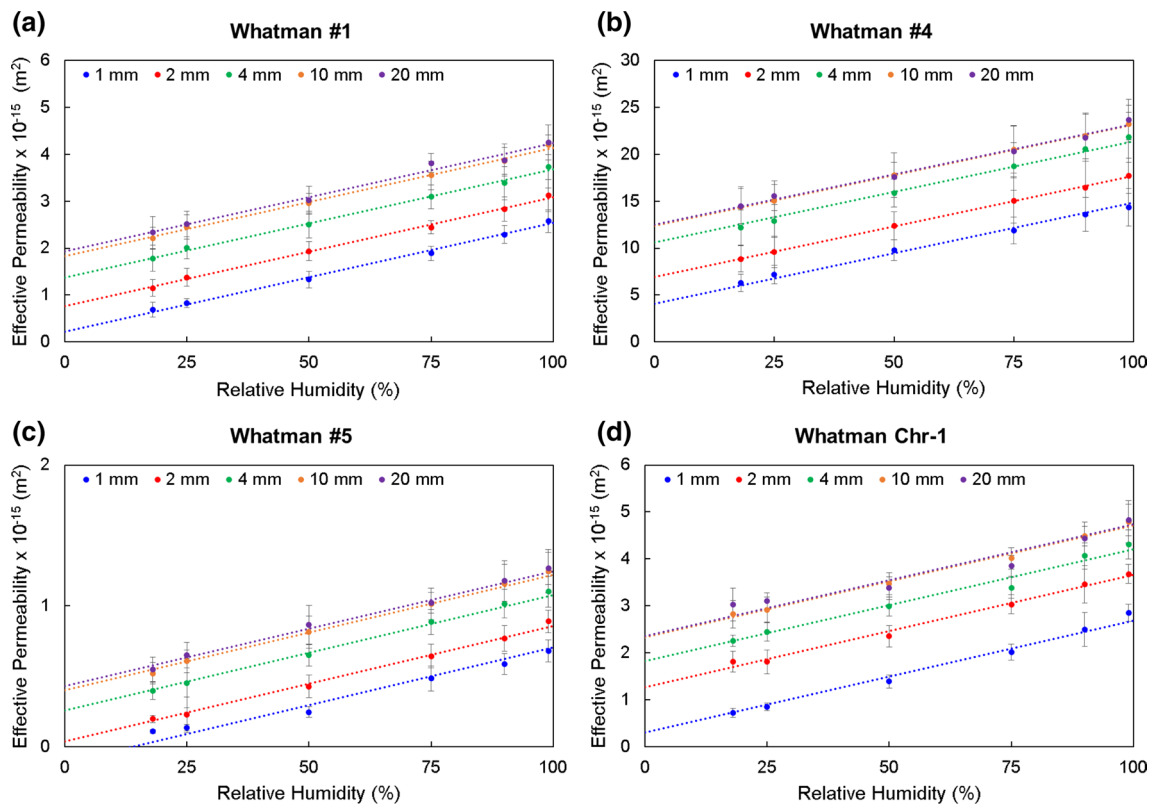


Fig. 7 Effective permeability versus relative humidity of surveyed paper types for the Fries et al. model. **a** Whatman #1, **b** Whatman #4, **c** Whatman #5, and **d** Whatman Chr-1. Dotted lines are best-fit lines with a constant slope. Data points shown as mean \pm SD ($N = 10$)

Figure 9 shows the R^2 value (note difference in vertical axis) for all the permeabilities associated with the surveyed papers at selected relative humidity (for full set see electronic supplementary information). The relatively low R^2 value at low relative humidity for the L–W model reiterates its limitations associated with evaporation. Interestingly, as the relative imbibition speed of the paper decreases (e.g., slow imbibition in Whatman #5), the accuracy of the evaporation models also decreases with that of the L–W model being the most prominent, (Fig. 9c). On the other hand, the accuracy of these models increases as the channel width increases. Additionally, plots of the three models against experimental data for selected conditions are available in Fig. S13–S16 in electronic supplementary information. Collectively, this comparison shows a critical importance of treating the permeability and hence the effective pore diameter as a function of both relative humidity and channel geometry.

In comparing the water saturation model to the Fries et al. model, it is found that the effective permeability values are almost identical. This result can be foreseen by finding the ratio of the evaporation to the water saturation. At high relative humidity, evaporation is low, while water saturation is at its highest. At low relative humidity,

evaporation is high, while water saturation is at its lowest. Irrespective of the case, for these types of paper, the evaporation term dominates over the water saturation at a specified relative humidity. Therefore, for characterization purposes the degree of water saturation is found to be negligible, although water saturation might have a significant impact on other aspects in paper-based microfluidic devices (e.g., morphological changes, moisture sensitive chemistry, device handling, shelf life). These types of investigations are beyond the scope of this manuscript.

3.6 Additional discussion

The capillary models in this study assume parallel capillary tubes with no dependence on orientation. In this study, the surveyed paper orientation where selected at random although the cellulose fibers have been previously shown to have a specific orientation known as the machine direction (MD), along which the imbibition speed is the fastest (Elizalde et al. 2016; Walji and MacDonald 2016; Xu and Enomae 2014). Following the method employed by Elizalde et al. (2016), we surveyed a total of 100 pieces of Whatman #1 filter paper (10 pieces \times 10 sheets) and found that such a preferred direction is not uniform across even a

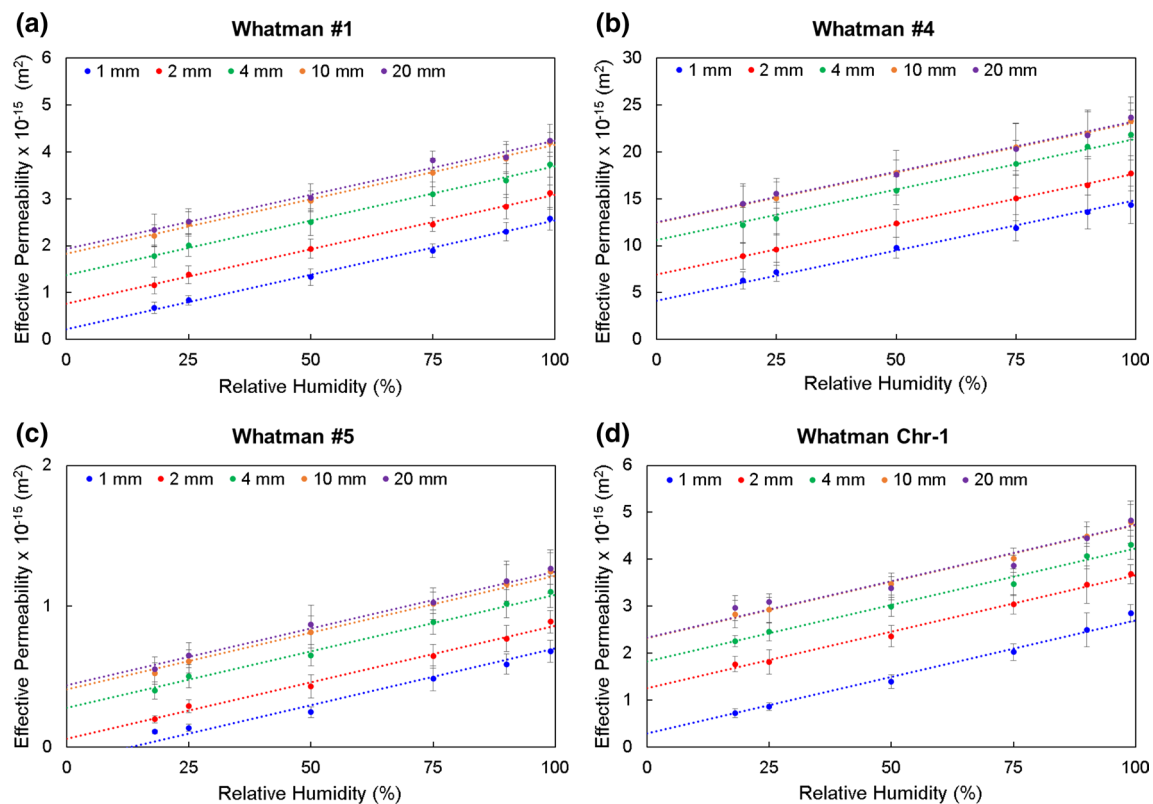
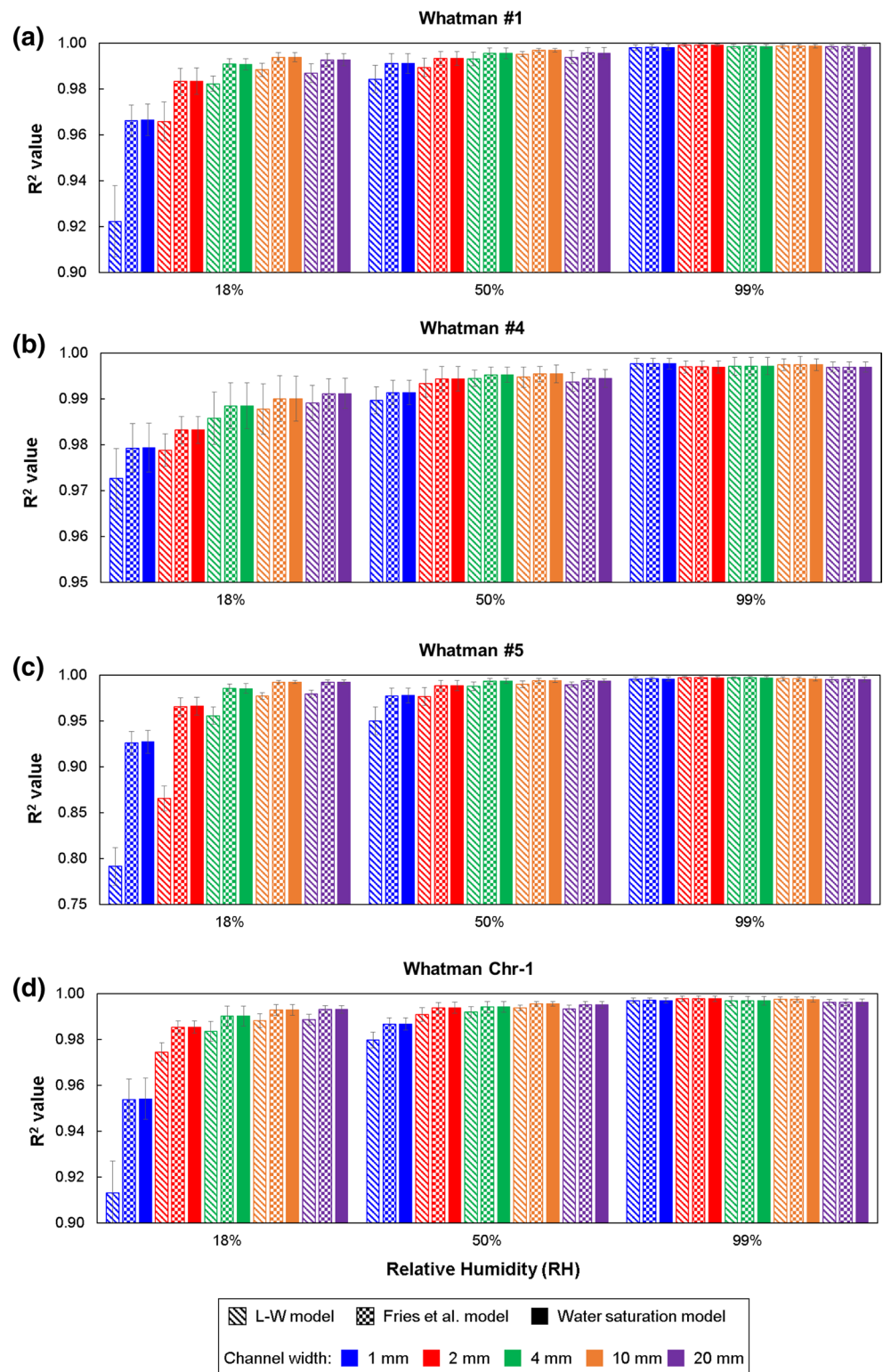


Fig. 8 Effective permeability versus relative humidity of surveyed paper types for the water saturation model. **a** Whatman #1, **b** Whatman #4, **c** Whatman #5, and **d** Whatman Chr-1. Dotted lines are best-fit lines with a constant slope. Data points shown as mean \pm SD ($N = 10$)

Fig. 9 R^2 values of effective permeability of surveyed paper types at selected relative humidity for L–W model, Fries et al. model, and the water saturation model. **a** Whatman #1, **b** Whatman #4, **c** Whatman #5, and **d** Whatman Chr-1. Data shown as mean \pm SD ($N = 10$)



single sheet of paper (Section S10 in electronic supplementary information). We next cut-out channels along the preferred wicking direction (0°), at 45° , and at 90° to estimate the effects of potential paper orientation. As shown in Fig. S19, difference in the wicking distances of these cases is

within error bars. Although additional investigations might help characterize the effects of paper orientation more in detail, these two experiments we conducted indicate the following; precisely selecting MD is impractical because it is not likely identical over the area of filter paper, and

its effect on the imbibition speed is reasonably small when compared with uncertainties due to other factors.

The current study used an adequately large reservoir of water, and all three models discussed here assume imbibition from an infinite reservoir. However, many practical applications of paper-based microfluidic devices are limited to a source of a finite volume. In most cases, this limited volume is enough to create a pseudo-infinite reservoir because the device is small enough or the flow is only important within a limited distance from the inlet. Nevertheless, future investigations on finite sources will be beneficial for liquid samples whose volume is extremely limited. Additionally, imbibition studies in channels made by other fabrication methods are expected to provide useful information toward designs of sophisticated paper-based microfluidic devices. In particular, many devices today are made by wax printing, ranging from the conventional open channels, to hemi-channels, and to fully enclosed channels (Renault et al. 2014). The hemi-channels and fully enclosed channels are closed on one side and both sides by the wax, respectively. Therefore, the reduced, exposed wet surfaces will reduce evaporation, aiding the imbibition process. On the other hand, as shown by Hong and Kim (2015), wax boundaries can inhibit the flow. Therefore, the resulting effects will depend on a balance between the increased flow resistance due to hydrophobic wax and the reduced evaporation.

4 Conclusions

In the current study, we characterized the effect of relative humidity and channel width on imbibition for paper-based microfluidic applications. The significant role of relative humidity on imbibition was demonstrated, as well as the impact of channel width on imbibition. Whereas the latter observation is in agreement with the result of Walji and MacDonald (2016), the former appears to contradict their observation that the effect of humidity on the imbibition speed was not noticeable. Comparing the L–W model to the evaporation models showed the ineffectiveness of the former in accurately describing flows at low relative humidity. In addition, comparison of the water saturation model to the Fries et al. model showed the water saturation term to be negligible for characterizing the fluid front. The strong interdependence of different parameters (relative humidity, channel width, paper type) has left the paper-based microfluidic device designers with an optimization challenge. Practical tools to accurately describe fluid transport in paper devices will become increasingly important as the designs of the devices evolve from 1-D to 3-D (Han et al. 2016; Kalish and Tsutsui 2014, 2016; Li and Liu 2014; Liu and Crooks 2011; Martinez et al. 2008a) as

well as incorporate advanced timing (Chen et al. 2012; Fu et al. 2012; Toley et al. 2013, 2015) and demultiplexing/multiplexing functions (Cate et al. 2015b; Lopez-Marzo and Merkoci 2016). The current study has created a library of paper-specific properties (e.g., water saturation, evaporation flux, effective permeability) for common cellulose papers used in the field of paper-based microfluidics. Effective use of this information will allow researchers to design more precise and reproducible paper-based microfluidic devices.

Acknowledgements This work was supported by the National Science Foundation under Grant No. CBET-1606181. Any opinions, findings, and conclusions expressed in this paper are those of the authors and do not necessarily reflect the views of the National Science Foundation. C. Castro acknowledges a fellowship from the California Space Grant Consortium. The authors would like to thank Brent Kalish for assistance with scanning electron microscopy.

References

- Abe K, Kotera K, Suzuki K, Citterio D (2010) Inkjet-printed paper-fluidic immuno-chemical sensing device. *Anal Bioanal Chem* 398:885–893. doi:[10.1007/s00216-010-4011-2](https://doi.org/10.1007/s00216-010-4011-2)
- Alava M, Dube M, Rost M (2004) Imbibition in disordered media. *Adv Phys* 53:83–175. doi:[10.1080/00018730410001687363](https://doi.org/10.1080/00018730410001687363)
- Amaral LAN, Barabasi AL, Buldyrev SV, Harrington ST, Havlin S, Sadrilahijany R, Stanley HE (1995) Avalanches and the directed percolation depinning model—experiments, simulations, and theory. *Phys Rev E* 51:4655–4673. doi:[10.1103/PhysRevE.51.4655](https://doi.org/10.1103/PhysRevE.51.4655)
- Apilux A, Ukita Y, Chikae M, Chailapakul O, Takamura Y (2013) Development of automated paper-based devices for sequential multistep sandwich enzyme-linked immunosorbent assays using inkjet printing. *Lab Chip* 13:126–135. doi:[10.1039/c2lc40690j](https://doi.org/10.1039/c2lc40690j)
- Balankin AS, Lopez HZ, Leon EP, Matamoros DM, Ruiz LM, Lopez DS, Rodriguez MA (2013) Depinning and dynamics of imbibition fronts in paper under increasing ambient humidity. *Phys Rev E*. doi:[10.1103/PhysRevE.87.014102](https://doi.org/10.1103/PhysRevE.87.014102)
- Ballerini, Li X, Shen W (2011) Flow control concepts for thread-based microfluidic devices. *Biomicrofluidics*. doi:[10.1063/1.3567094](https://doi.org/10.1063/1.3567094)
- Berli CLA, Kler PA (2016) A quantitative model for lateral flow assays. *Microfluid Nanofluid*. doi:[10.1007/s10404-016-1771-9](https://doi.org/10.1007/s10404-016-1771-9)
- Bledzki AK, Gassan J (1999) Composites reinforced with cellulose based fibres. *Prog Polym Sci* 24:221–274. doi:[10.1016/S0079-6700\(98\)00018-5](https://doi.org/10.1016/S0079-6700(98)00018-5)
- Bohm A, Carstens F, Trieb C, Schabel S, Biesalski M (2014) Engineering microfluidic papers: effect of fiber source and paper sheet properties on capillary-driven fluid flow. *Microfluid Nanofluid* 16:789–799. doi:[10.1007/s10404-013-1324-4](https://doi.org/10.1007/s10404-013-1324-4)
- Carrilho E, Martinez AW, Whitesides GM (2009) Understanding wax printing: a simple micropatterning process for paper-based microfluidics. *Anal Chem* 81:7091–7095. doi:[10.1021/ac901071p](https://doi.org/10.1021/ac901071p)
- Cate DM, Adkins JA, Mettakoonpitak J, Henry CS (2015a) Recent developments in paper-based microfluidic devices. *Anal Chem* 87:19–41. doi:[10.1021/ac503968p](https://doi.org/10.1021/ac503968p)
- Cate DM, Noblitt SD, Volckens J, Henry CS (2015b) Multiplexed paper analytical device for quantification of metals using distance-based detection. *Lab Chip* 15:2808–2818. doi:[10.1039/c5lc00364d](https://doi.org/10.1039/c5lc00364d)

- Chen H, Cogswell J, Anagnostopoulos C, Faghri M (2012) A fluidic diode, valves, and a sequential-loading circuit fabricated on layered paper. *Lab Chip* 12:2909–2913. doi:[10.1039/C2lc20970e](https://doi.org/10.1039/C2lc20970e)
- Chitnis G, Ding ZW, Chang CL, Savran CA, Ziaie B (2011) Laser-treated hydrophobic paper: an inexpensive microfluidic platform. *Lab Chip* 11:1161–1165. doi:[10.1039/c0lc00512f](https://doi.org/10.1039/c0lc00512f)
- Connelly JT, Rolland JP, Whitesides GM (2015) “Paper machine” for molecular diagnostics. *Anal Chem* 87:7595–7601. doi:[10.1021/acs.analchem.5b00411](https://doi.org/10.1021/acs.analchem.5b00411)
- Elizalde E, Urteaga R, Berli CLA (2015) Rational design of capillary-driven flows for paper-based microfluidics. *Lab Chip* 15:2173–2180. doi:[10.1039/c4lc01487a](https://doi.org/10.1039/c4lc01487a)
- Elizalde E, Urteaga R, Berli CLA (2016) Precise capillary flow for paper-based viscometry. *Microfluid Nanofluid*. doi:[10.1007/s10404-016-1800-8](https://doi.org/10.1007/s10404-016-1800-8)
- Fenton EM, Mascarenas MR, Lopez GP, Sibbett SS (2009) Multiplex lateral-flow test strips fabricated by two-dimensional shaping. *Acs Appl Mater Interfaces* 1:124–129. doi:[10.1021/Am800043z](https://doi.org/10.1021/Am800043z)
- Fridley GE, Le H, Yager P (2014) Highly sensitive immunoassay based on controlled rehydration of patterned reagents in a 2-dimensional paper network. *Anal Chem* 86:6447–6453. doi:[10.1021/ac500872j](https://doi.org/10.1021/ac500872j)
- Fries N, Odic K, Conrath M, Dreyer M (2008) The effect of evaporation on the wicking of liquids into a metallic weave. *J Colloid Interface Sci* 321:118–129. doi:[10.1016/J.Jcis.2008.01.019](https://doi.org/10.1016/J.Jcis.2008.01.019)
- Fu E, Kauffman P, Lutz B, Yager P (2010) Chemical signal amplification in two-dimensional paper networks. *Sens Actuators B Chem* 149:325–328. doi:[10.1016/J.Snb.2010.06.024](https://doi.org/10.1016/J.Snb.2010.06.024)
- Fu EL, Ramsey S, Kauffman P, Lutz B, Yager P (2011) Transport in two-dimensional paper networks. *Microfluid Nanofluid* 10:29–35. doi:[10.1007/S10404-010-0643-Y](https://doi.org/10.1007/S10404-010-0643-Y)
- Fu E, Liang T, Spicar-Mihalic P, Houghtaling J, Ramachandran S, Yager P (2012) Two-dimensional paper network format that enables simple multistep assays for use in low-resource settings in the context of malaria antigen detection. *Anal Chem* 84:4574–4579. doi:[10.1021/Ac300689s](https://doi.org/10.1021/Ac300689s)
- Giokas DL, Tsogas GZ, Vlessidis AG (2014) Programming fluid transport in paper-based microfluidic devices using razor-crafted open channels. *Anal Chem* 86:6202–6207. doi:[10.1021/ac501273v](https://doi.org/10.1021/ac501273v)
- Han KN, Choi JS, Kwon J (2016) Three-dimensional paper-based slip device for one-step point-of-care testing. *Sci Rep*. doi:[10.1038/Srep25710](https://doi.org/10.1038/Srep25710)
- Hong S, Kim W (2015) Dynamics of water imbibition through paper channels with wax boundaries. *Microfluid Nanofluid* 19:845–853. doi:[10.1007/s10404-015-1611-3](https://doi.org/10.1007/s10404-015-1611-3)
- Jahanshahi-Anbuhi S et al (2014) Paper-based microfluidics with an erodible polymeric bridge giving controlled release and timed flow shutoff. *Lab Chip* 14:229–236. doi:[10.1039/c3lc50762a](https://doi.org/10.1039/c3lc50762a)
- Jiang X, Fan ZH (2016) Fabrication and operation of paper-based analytical devices. *Annu Rev Anal Chem* 9:203–222. doi:[10.1146/annurev-anchem-071015-041714](https://doi.org/10.1146/annurev-anchem-071015-041714)
- Kalish B, Tsutsui H (2014) Patterned adhesive enables construction of nonplanar three-dimensional paper microfluidic circuits. *Lab Chip* 14:4354–4361. doi:[10.1039/c4lc00730a](https://doi.org/10.1039/c4lc00730a)
- Kalish B, Tsutsui H (2016) Using adhesive patterning to construct 3D paper microfluidic devices. *J Vis Exp*. doi:[10.3791/53805](https://doi.org/10.3791/53805)
- Kardar M, Parisi G, Zhang YC (1986) Dynamic scaling of growing interfaces. *Phys Rev Lett* 56:889–892. doi:[10.1103/PhysRevLett.56.889](https://doi.org/10.1103/PhysRevLett.56.889)
- Kauffman P, Fu E, Lutz B, Yager P (2010) Visualization and measurement of flow in two-dimensional paper networks. *Lab Chip* 10:2614–2617. doi:[10.1039/C004766j](https://doi.org/10.1039/C004766j)
- Krug J, Meakin P (1991) Kinetic roughening of Laplacian fronts. *Phys Rev Lett* 66:703–706. doi:[10.1103/PhysRevLett.66.703](https://doi.org/10.1103/PhysRevLett.66.703)
- Li X, Liu XY (2014) Fabrication of three-dimensional microfluidic channels in a single layer of cellulose paper. *Microfluid Nanofluid* 16:819–827. doi:[10.1007/s10404-014-1340-z](https://doi.org/10.1007/s10404-014-1340-z)
- Li X, Tian JF, Garnier G, Shen W (2010) Fabrication of paper-based microfluidic sensors by printing. *Colloids Surf B* 76:564–570. doi:[10.1016/J.Colsurfb.2009.12.023](https://doi.org/10.1016/J.Colsurfb.2009.12.023)
- Liu H, Crooks RM (2011) Three-dimensional paper microfluidic devices assembled using the principles of origami. *J Am Chem Soc* 133:17564–17566. doi:[10.1021/Ja2071779](https://doi.org/10.1021/Ja2071779)
- Liukkonen A (1997) Contact angle of water on paper components: sessile drops versus environmental scanning electron microscope measurements. *Scanning* 19:411–415
- Lopez-Marzo AM, Merkoci A (2016) Paper-based sensors and assays: a success of the engineering design and the convergence of knowledge areas. *Lab Chip*. doi:[10.1039/c6lc00737f](https://doi.org/10.1039/c6lc00737f)
- Lucas R (1918) The time law of the capillary rise of liquids. *Kolloid Zeitschrift* 23:15–22. doi:[10.1007/Bf01461107](https://doi.org/10.1007/Bf01461107)
- Lutz B, Liang T, Fu E, Ramachandran S, Kauffman P, Yager P (2013) Dissolvable fluidic time delays for programming multi-step assays in instrument-free paper diagnostics. *Lab Chip* 13:2840–2847. doi:[10.1039/c3lc50178g](https://doi.org/10.1039/c3lc50178g)
- Martinez AW, Phillips ST, Butte MJ, Whitesides GM (2007) Patterned paper as a platform for inexpensive, low-volume, portable bioassays. *Angew Chem Int Ed* 46:1318–1320. doi:[10.1002/Anie.200603817](https://doi.org/10.1002/Anie.200603817)
- Martinez AW, Phillips ST, Whitesides GM (2008a) Three-dimensional microfluidic devices fabricated in layered paper and tape. *Proc Natl Acad Sci USA* 105:19606–19611. doi:[10.1073/pnas.0810903105](https://doi.org/10.1073/pnas.0810903105)
- Martinez AW, Phillips ST, Wiley BJ, Gupta M, Whitesides GM (2008b) FLASH: a rapid method for prototyping paper-based microfluidic devices. *Lab Chip* 8:2146–2150. doi:[10.1039/b811135a](https://doi.org/10.1039/b811135a)
- Masoodi R, Pillai KM (2010) Darcy’s law-based model for wicking in paper-like swelling porous media. *AIChE J* 56:2257–2267. doi:[10.1002/Aic.12163](https://doi.org/10.1002/Aic.12163)
- Mendez S et al (2010) Imbibition in porous membranes of complex shape: quasi-stationary flow in thin rectangular segments. *Langmuir* 26:1380–1385. doi:[10.1021/La902470b](https://doi.org/10.1021/La902470b)
- Moon RJ, Martini A, Nairn J, Simonsen J, Youngblood J (2011) Cellulose nanomaterials review: structure, properties and nanocomposites. *Chem Soc Rev* 40:3941–3994. doi:[10.1039/C0cs00108b](https://doi.org/10.1039/C0cs00108b)
- Noh N, Phillips ST (2010) Metering the capillary-driven flow of fluids in paper-based microfluidic devices. *Anal Chem* 82:4181–4187. doi:[10.1021/ac100431y](https://doi.org/10.1021/ac100431y)
- Park J, Shin JH, Park JK (2016) Experimental analysis of porosity and permeability in pressed paper. *Micromachines*. doi:[10.3390/mi7030048](https://doi.org/10.3390/mi7030048)
- Renault C, Li X, Fosdick SE, Crooks RM (2013) Hollow-channel paper analytical devices. *Anal Chem* 85:7976–7979. doi:[10.1021/ac401786h](https://doi.org/10.1021/ac401786h)
- Renault C, Koehne J, Ricco AJ, Crooks RM (2014) Three-dimensional wax patterning of paper fluidic devices. *Langmuir* 30:7030–7036. doi:[10.1021/la501212b](https://doi.org/10.1021/la501212b)
- Richards LA (1931) Capillary conduction of liquids through porous mediums. *Physics J Gen Appl P* 1:318–333. doi:[10.1063/1.1745010](https://doi.org/10.1063/1.1745010)
- Schuchardt DR, Berg JC (1991) Liquid transport in composite cellulose—superabsorbent fiber networks. *Wood Fiber Sci* 23:342–357
- Shou DH, Ye L, Fan JT, Fu KK, Mei MF, Wang HJ, Chen Q (2014) Geometry-induced asymmetric capillary flow. *Langmuir* 30:5448–5454. doi:[10.1021/la500479e](https://doi.org/10.1021/la500479e)
- Songok J, Salminen P, Toivakka M (2014) Temperature effects on dynamic water absorption into paper. *J Colloid Interface Sci* 418:373–377. doi:[10.1016/j.jcis.2013.12.017](https://doi.org/10.1016/j.jcis.2013.12.017)

- Toley BJ, McKenzie B, Liang T, Buser JR, Yager P, Fu E (2013) Tunable-delay shunts for paper microfluidic devices. *Anal Chem* 85:11545–11552. doi:[10.1021/Ac4030939](https://doi.org/10.1021/Ac4030939)
- Toley BJ et al (2015) A versatile valving toolkit for automating fluidic operations in paper microfluidic devices. *Lab Chip* 15:1432–1444. doi:[10.1039/c4lc01155d](https://doi.org/10.1039/c4lc01155d)
- Walji N, MacDonald BD (2016) Influence of geometry and surrounding conditions on fluid flow in paper-based devices. *Micromachines*. doi:[10.3390/Mi7050073](https://doi.org/10.3390/Mi7050073)
- Washburn EW (1921) The dynamics of capillary flow. *Phys Rev* 17:273–283. doi:[10.1103/Physrev.17.273](https://doi.org/10.1103/Physrev.17.273)
- Weng CH, Chen MY, Shen CH, Yang RJ (2014) Colored wax-printed timers for two-dimensional and three-dimensional assays on paper-based devices. *Biomicrofluidics*. doi:[10.1063/1.4902246](https://doi.org/10.1063/1.4902246)
- Xia Y, Si J, Li Z (2016) Fabrication techniques for microfluidic paper-based analytical devices and their applications for biological testing: a review. *Biosens Bioelectron* 77:774–789. doi:[10.1016/j.bios.2015.10.032](https://doi.org/10.1016/j.bios.2015.10.032)
- Xu Y, Enomae T (2014) Paper substrate modification for rapid capillary flow in microfluidic paper-based analytical devices. *Rsc Adv* 4:12867–12872. doi:[10.1039/c4ra00434e](https://doi.org/10.1039/c4ra00434e)
- Yetisen AK, Akram MS, Lowe CR (2013) Paper-based microfluidic point-of-care diagnostic devices. *Lab Chip* 13:2210–2251. doi:[10.1039/c3lc50169h](https://doi.org/10.1039/c3lc50169h)